PNAS

Supporting Information for

Actions of the Anti-Seizure Drug Carbamazepine in the Thalamic Reticular Nucleus: Potential Mechanism of Aggravating Absence Seizures

Sung-Soo Jang, Nicole Agranonik, John R. Huguenard*

John R Huguenard
Email: huguenard@stanford.edu

This PDF file includes:

Figures S1 to S12

Supplemental Material and Methods

Reference

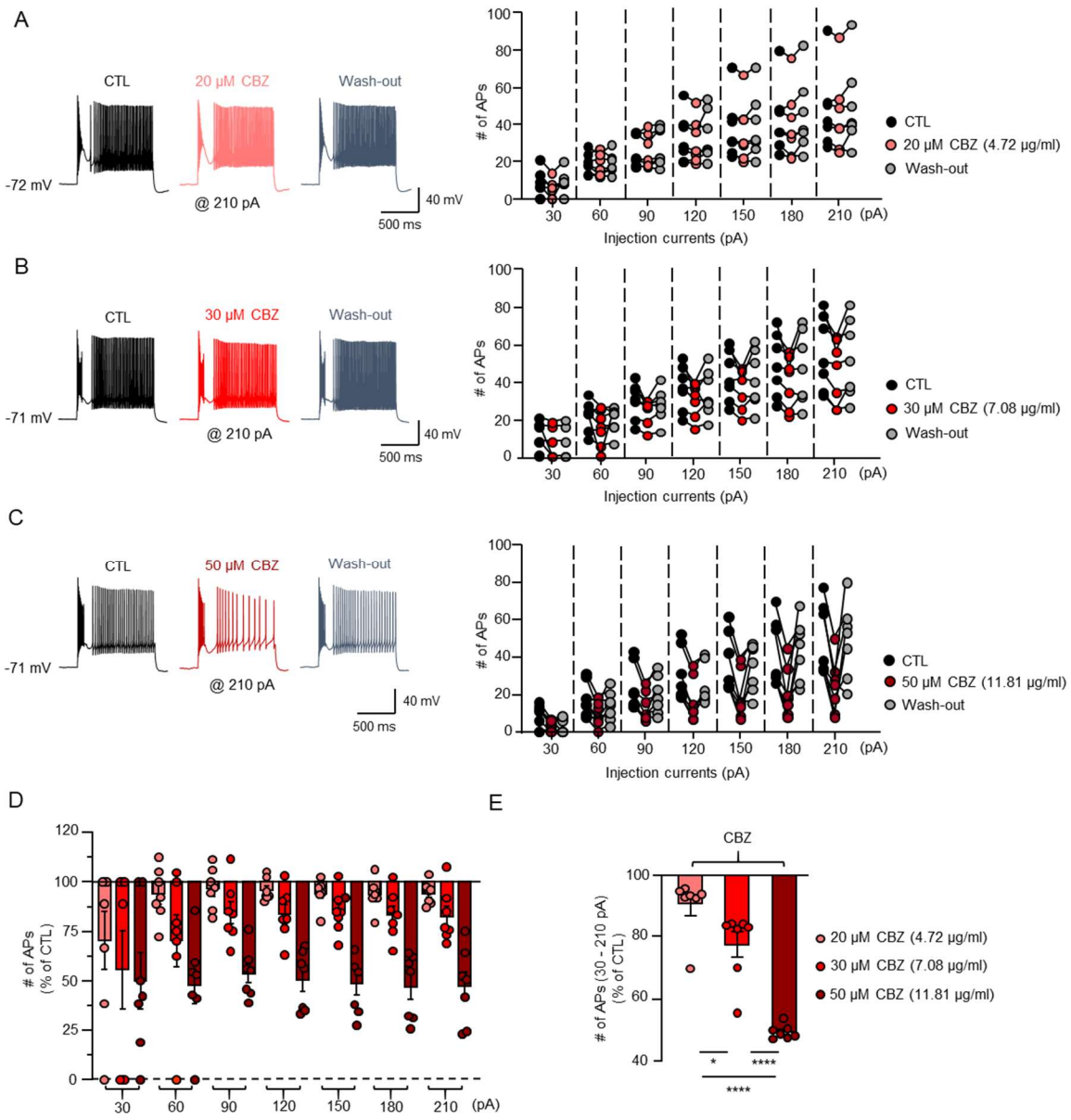

Fig. S1. Dose-Dependent Inhibition of RT Neuronal Firing by CBZ. (A) Representative traces (left) showing AP trains elicited by 210 pA current injection from a holding potential of -72 mV and graph (right) showing the number of APs elicited by current injections (30 – 210 pA, in 30 pA increments) for 1-second during CTL, 20 μM CBZ, and wash-out (n = 7). (B) Representative traces (left) showing AP trains elicited by 210 pA current injection from a holding potential of -71 mV and graph (right) showing the number of APs elicited by current injections (30 – 210 pA, in 30 pA increments) for 1-second during CTL, 30 μM CBZ, and wash-out (n = 7). (C) Representative traces (left) showing AP trains elicited by 210 pA current injection from a holding potential of -71 mV and graph (right) showing the number of APs elicited by current injections (30 – 210 pA, in 30 pA increments) for 1-second during CTL, 50 μM CBZ, and wash-out (n = 7). (D) Graph showing the normalized percentage reduction in the number of APs elicited by current injections ranging from 30 to 210 pA across three different CBZ concentrations (20, 30, and 50 μM). (E) Summary graph displaying normalized number of APs to CTL at 20 μM (n = 7), 30 μM (n = 7), and 50 μM (n = 7) CBZ. Statistical significance was determined using one-way ANOVA test. *p < 0.05, ****p < 0.0001.

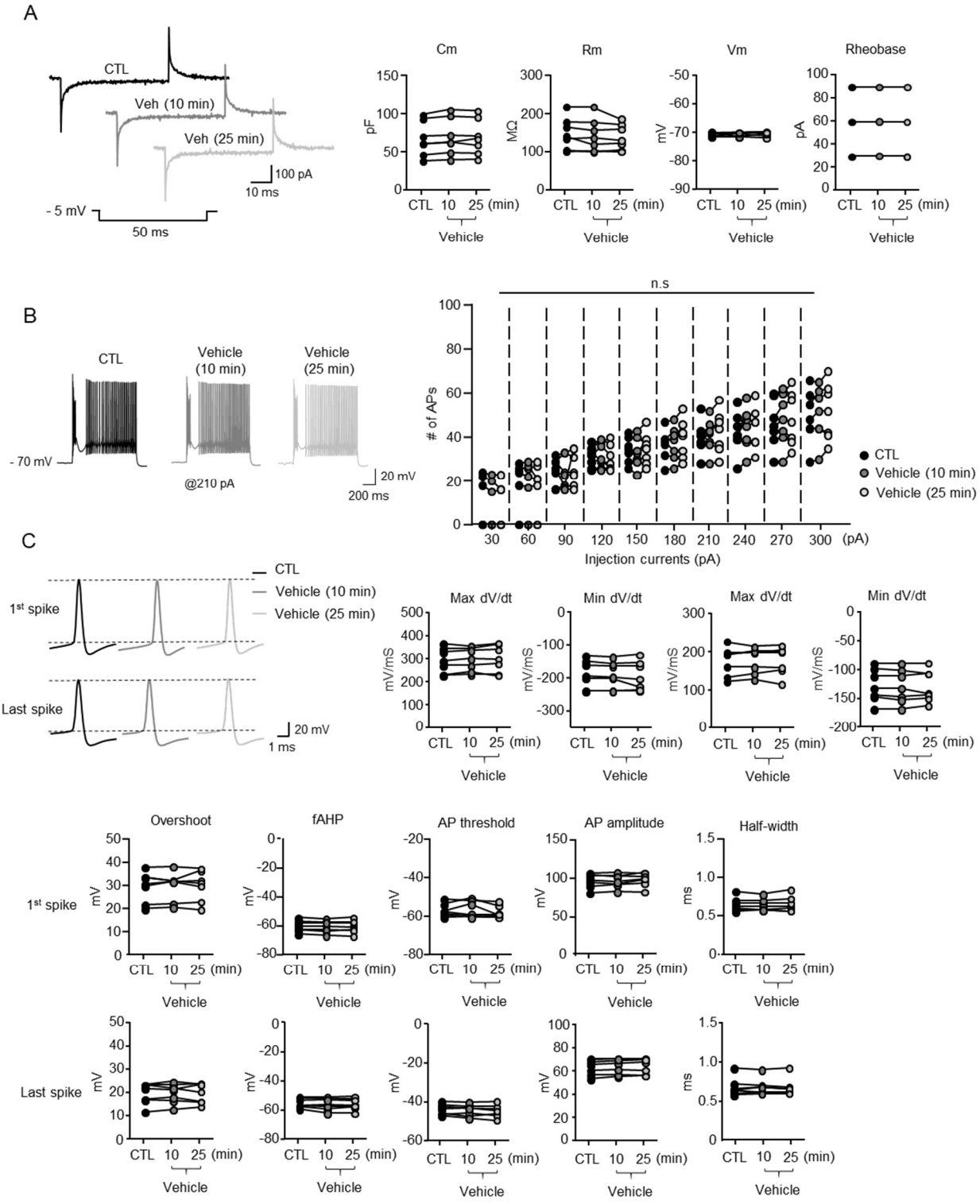

Fig. S2. No Changes in Passive, Action Potential, and Action Potential Properties in RT Neurons during CTL, Vehicle (10 and 25 min). (A) Representative traces (left) showing the current elicited by – 5 mV pulse recorded during CTL and vehicle (10 and 25 min) conditions and graphs (right) displaying the

values of capacitance (pF), membrane resistance (MΩ), membrane voltage (mV), and rheobase (pA). (B) Representative traces (left) showing AP trains elicited by 210 pA current injection from a holding potential of -70 mV and graph (right) showing the number of APs elicited by current injections (30 – 300 pA, in 30 pA increments) for 1 second during CTL and vehicle (10 and 25 min) (n = 7). (C) Representative traces (left) showing the first and last APs elicited by 300 pA current injection from a holding potential of -70 mV recorded during CTL and vehicle (10 and 25 min) conditions and graphs (right, top and bottom) displaying the average values of AP parameters, including overshoot, fast afterhyperpolarization (fAHP), half-width, AP threshold, and AP amplitude, measured from the first and last spikes (n = 7). Statistical significance was determined using a paired t-test.

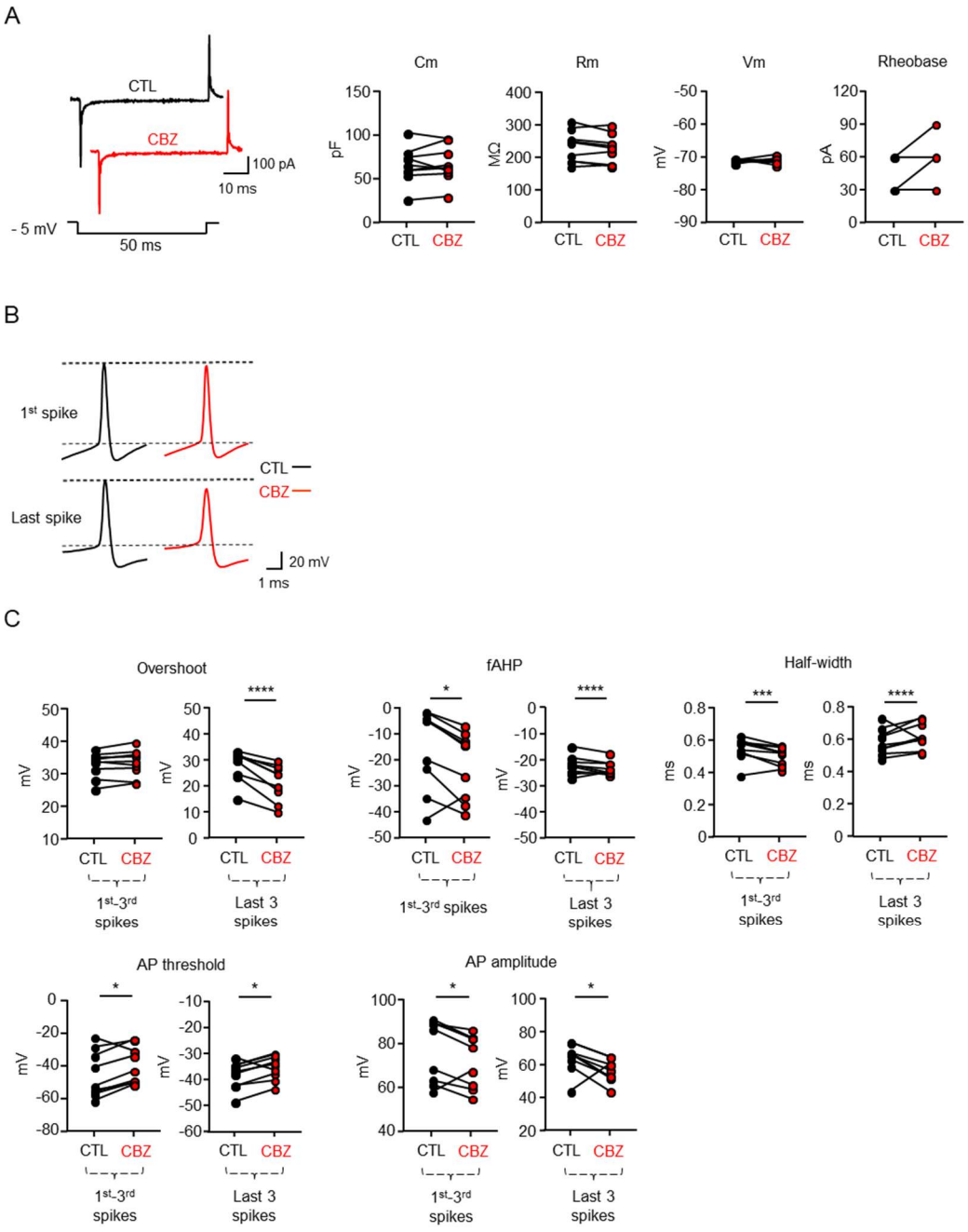

Fig. S3. Changes in Action Potential Properties in RT Neurons Following CBZ Treatment. (A) Representative traces (left) showing the current elicited by – 5 mV pulse recorded before and after CBZ incubation and graphs (right) displaying the values of capacitance (pF), membrane resistance (MΩ), membrane voltage (mV), and rheobase (pA). (B) Representative traces showing the first and last spikes elicited by 300 pA current injection recorded before and after CBZ incubation. (C) Graphs showing the values of AP parameters, including overshoot, fast afterhyperpolarization (fAHP), half-width, AP threshold, and AP amplitude, quantified from the 1st–3rd spikes and the last 3 spikes during the current injection (n = 9). Statistical significance was determined using a paired t-test. *p < 0.05, ***p < 0.001, ****p < 0.0001.

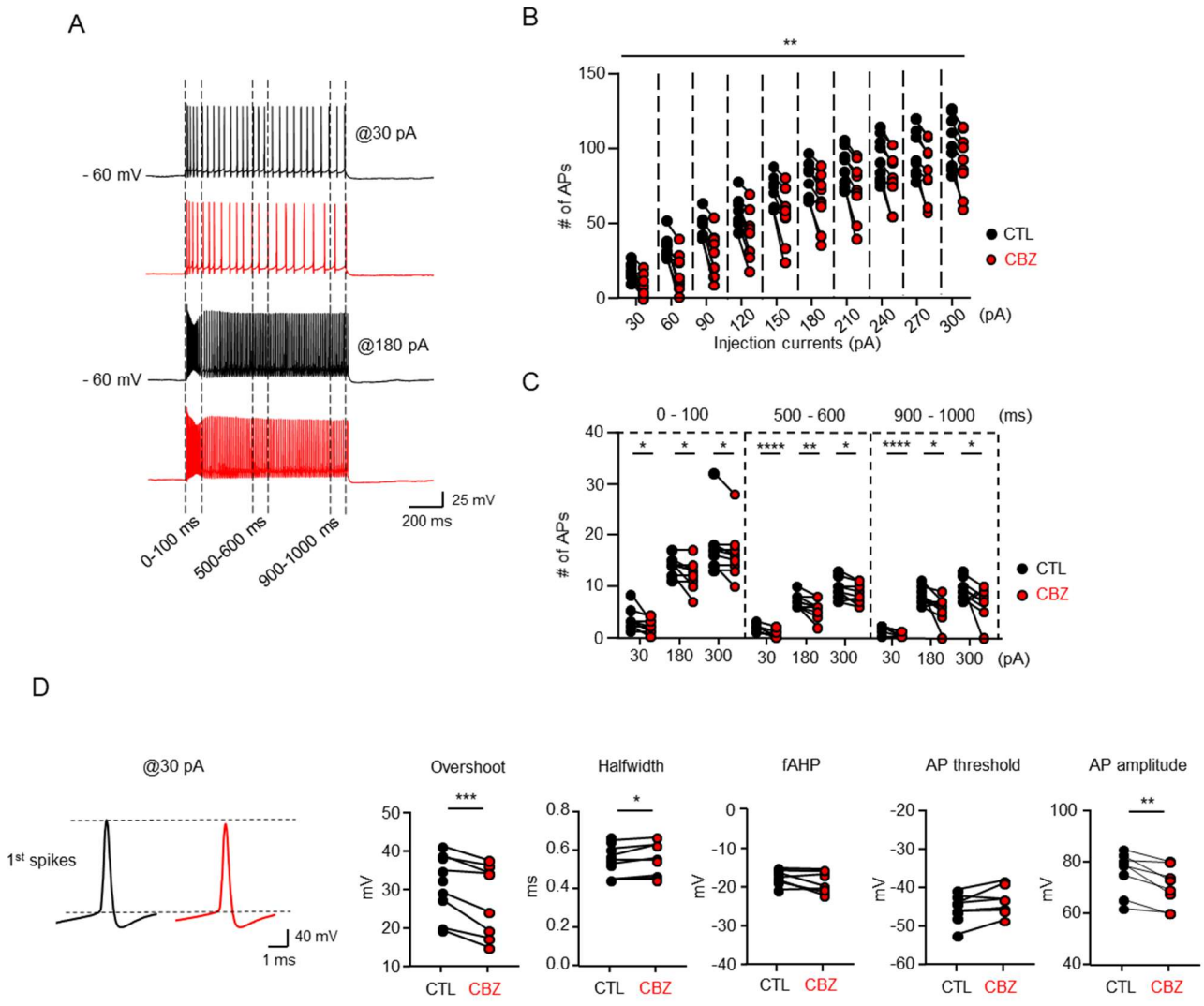

Fig. S4. Inhibition of Tonic Firing in RT Neurons by CBZ. (A) Representative traces showing tonic firing elicited by 30 pA and 180 pA current injections from a holding potential of -60 mV, recorded before (black) and after (red) a 10-minute incubation with 30 μM CBZ (n = 9). (B) Graph showing the number of APs elicited by current injections ranging from 0 to 300 pA (in 30 pA increments) for 1-second. (C) Graph showing the number of APs at specific time intervals (0–100 ms, 500–600 ms, and 900–1000 ms) elicited by current injections of 30, 180, and 300 pA for 1-second. (D) Representative traces (left) showing the first AP elicited by 30 pA current injection at a holding potential of -60 mV and graphs (right) showing the values of AP parameters, including overshoot, fast afterhyperpolarization (fAHP), half-width, AP threshold, and AP amplitude of the first spikes before and after CBZ incubation. Statistical analysis was performed using a paired t-test. *p < 0.05, **p < 0.01, ***p < 0.001, ****p < 0.0001.

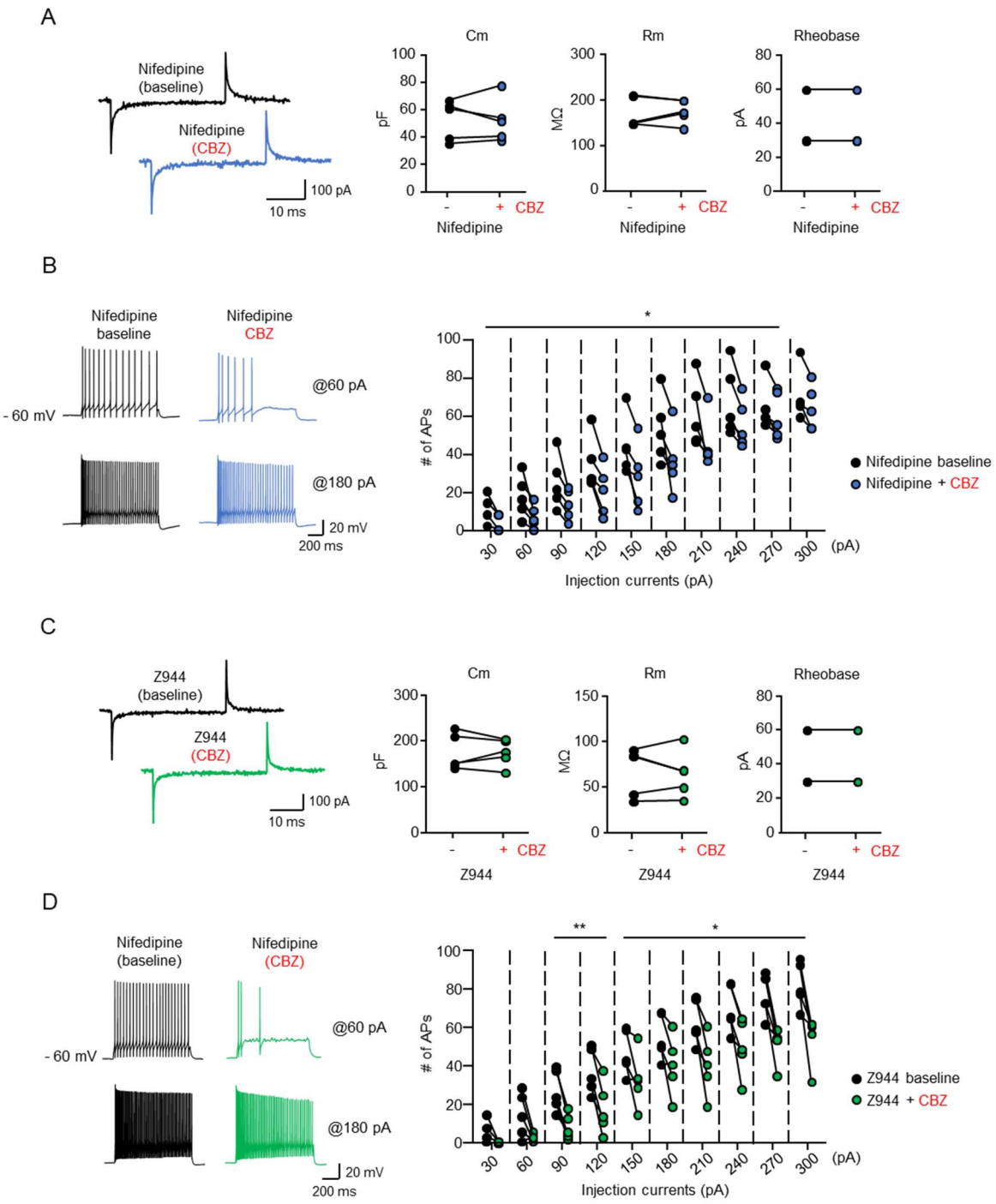

Fig. S5. Nifedipine (L-type calcium channel) and Z944 (T-type calcium channel) do not affect inhibition of tonic firing in RT Neurons by CBZ. (A) Representative traces (left) showing the current elicited by –5 mV pulse recorded during nifedipine (10 μM, baseline) and nifedipine (10 μM) with CBZ incubation and graphs (right) displaying the values of capacitance (pF), membrane resistance (MΩ), and Rheobase (pA). (B) Representative traces (left) showing AP trains elicited by 210 pA current injection from a holding potential of -60 mV and graph (right) showing the number of APs elicited by current injections (30 – 300 pA, in 30 pA increments) for 1-second during nifedipine (10 μM, baseline) and nifedipine (10 μM) with CBZ incubation (n = 5). (C) Representative traces (left) showing the current elicited by – 5 mV pulse from

a holding potential of -60 mV recorded during Z944 (5 μM, baseline) and Z944 (5 μM) with CBZ incubation and graphs (right) showing the values of capacitance (pF), membrane resistance (MΩ), and Rheobase (pA). (D) Representative traces (left) showing AP trains elicited by 210 pA current injection from a holding potential of -60 mV and graph (right) showing the number of APs elicited by current injections (30 – 300 pA, in 30 pA increments) for 1-second during Z944 (5 μM, baseline) and Z944 (5 μM) with CBZ incubation (n = 5). Statistical analysis was performed using a paired t-test. *$p < 0.05$, **$p < 0.01$.

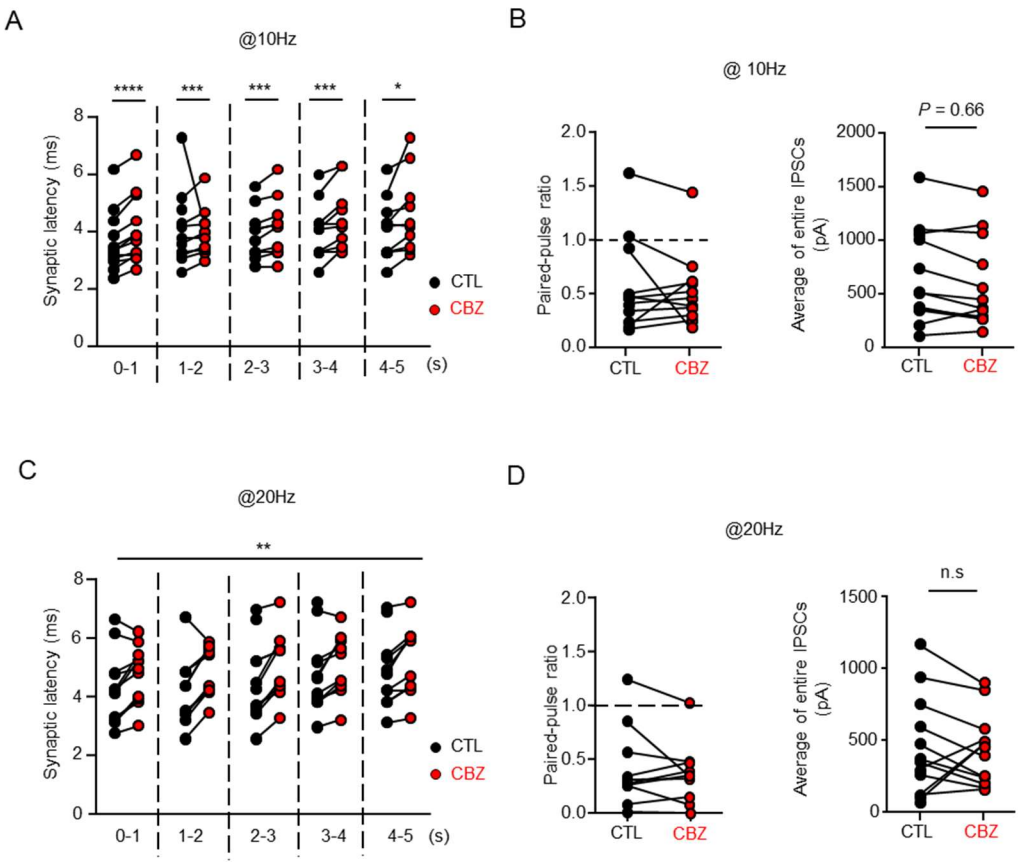

Fig. S6. CBZ-Induced Alterations in Synaptic Latency at 10 and 20 Hz Stimulation in VGAT-ChR2 mice. (A) Graph showing synaptic latency measured at 1-second intervals in response to 10 Hz optogenetic stimulation before and after CBZ incubation (n = 12). (B) Graph (left) displaying the PPR, calculated as the ratio of the 2nd to 1st IPSC peak amplitudes and graph (right) showing average of entire IPSCs during 10 Hz stimulation before and after CBZ incubation. (C) Graph showing synaptic latency measured at 1-second intervals in response to 20 Hz optogenetic stimulation before and after CBZ incubation (n = 12). (D) Graph (left) displaying the PPR, calculated as the ratio of the 2nd to 1st IPSC peak amplitudes and graph (right) displaying average of entire IPSCs during 20 Hz stimulation before and after CBZ incubation. Statistical significance was determined using a paired t-test. *p < 0.05, **p < 0.01, ***p < 0.001.

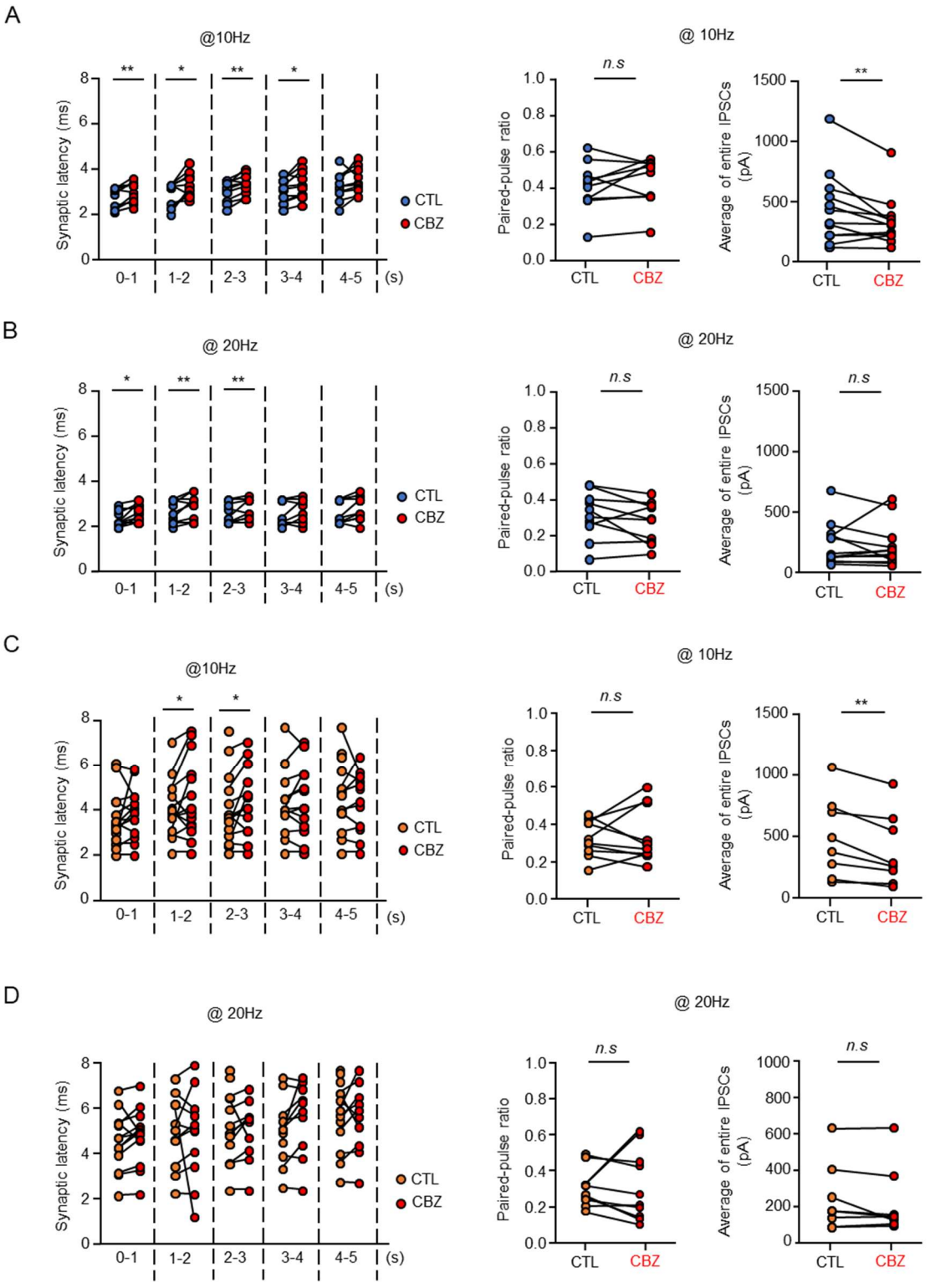

Fig. S7. CBZ-Induced Alterations in Synaptic Latency at 10 and 20 Hz in PV-cre and SOM-cre Mice. (A-B) Graph (left) showing synaptic latency at 1-second intervals in response to 10 Hz, graph (middle) showing the PPR, calculated as the ratio of the 2nd to 1st IPSC peak amplitudes and graph (right) showing

average of entire IPSCs during 10 Hz (A) and 20 Hz (B) stimulation before and after CBZ incubation in PV-cre mice (n = 10). (C-D) graph (left) showing synaptic latency at 1-second intervals in response to 10 Hz, graph (middle) showing the PPR, calculated as the ratio of the 2^{nd} to 1^{st} IPSC peak amplitudes, and graph (right) showing average of entire IPSCs during 10 Hz (C) and 20 Hz (D) stimulation before and after CBZ incubation in SOM-cre mice (n = 13). Statistical significance was determined using a paired t-test. *$p < 0.05$, **$p < 0.01$.

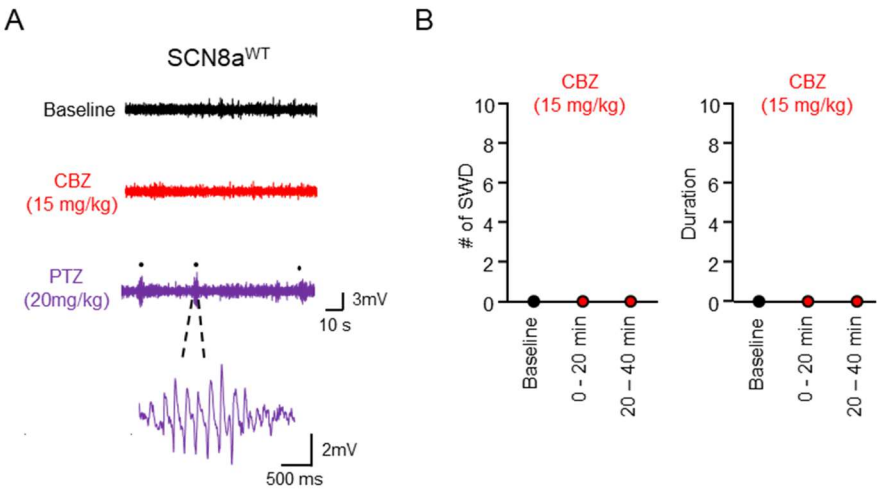

Fig. S8. Lack of CBZ-Induced Absence Seizures in SCN8a^{WT} Mice. (A) Representative EEG traces in SCN8a^{WT} mice during baseline, after CBZ administration (15 mg/kg, i.p.), and following PTZ administration (20 mg/kg, i.p.). (B) Graphs showing the number and total duration of SWDs over a 60-minute recording period following CBZ (15 mg/kg, i.p.) administration (n = 5).

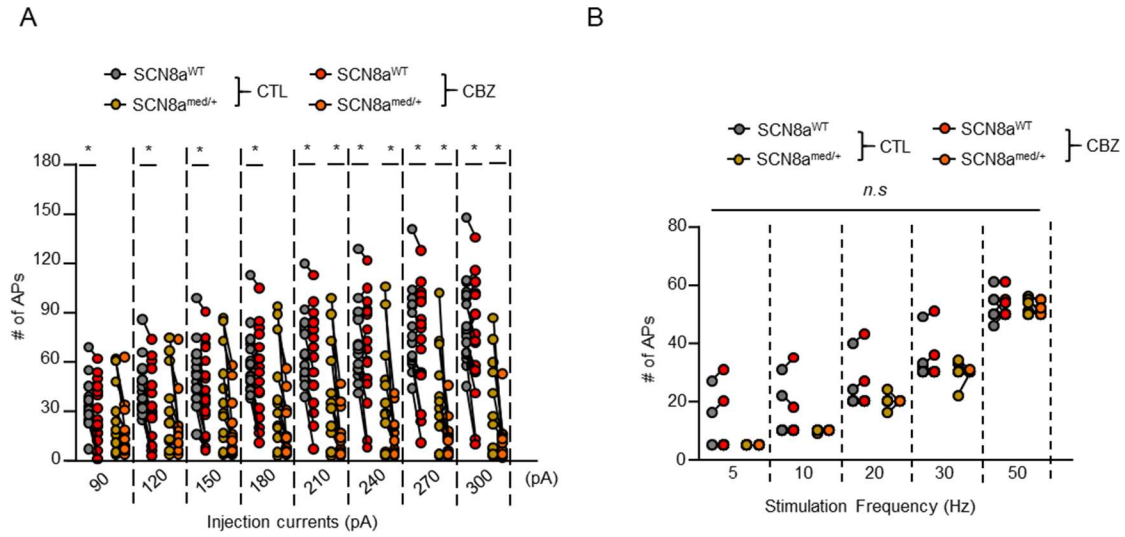

Fig. S9. Detailed data of APs altered by CBZ in RT neurons of SCN8a^{WT} and SCN8a$^{med/+}$ mice. (A) Graph showing the number of APs elicited by varying current injections (90 – 300 pA, in 30 pA increments) before and after CBZ incubation in SCN8a^{WT} (n = 15) and SCN8a$^{med/+}$ mice (n = 15). (B) Graph showing the number of APs elicited by 5, 10, 20, 30, and 50 Hz pulse trains before and after CBZ incubation in SCN8a^{WT} (n = 10) and SCN8a$^{med/+}$ mice (n = 9). Statistical significance was determined using a paired t-test. *p < 0.05.

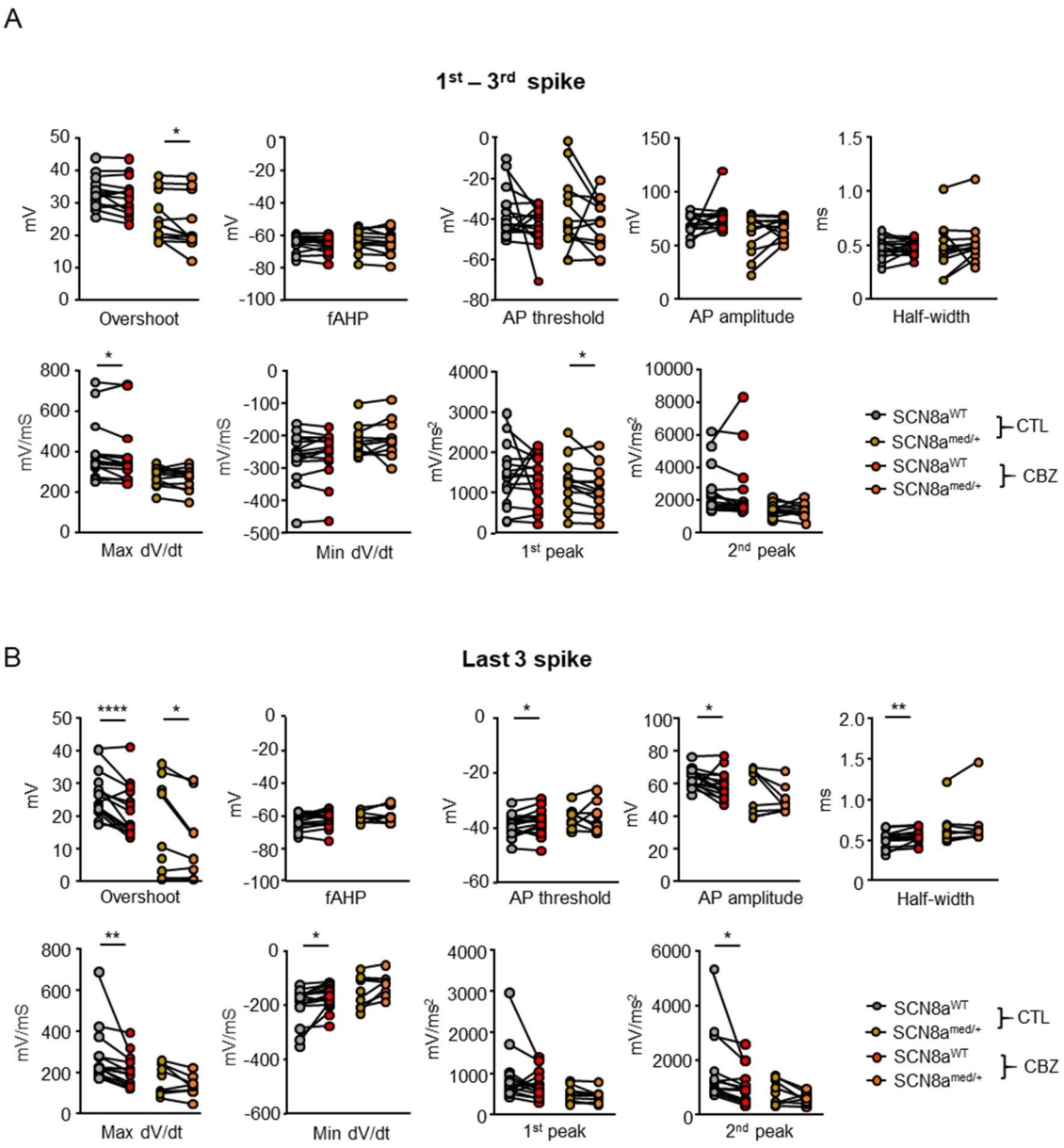

Fig. S10. CBZ-induced changes in parameters of AP elicited by DS pulse in RT Neurons. (A) Graphs showing changes in AP parameters (overshoot, fAHP, AP threshold, AP amplitude, half-width, maximum dV/dt, minimum dV/dt, and 1st/2nd peaks of d²V/dt²) for the 1st–3rd spikes elicited by 300 pA injections before and after CBZ incubation in SCN8a^{WT} (n = 15) and SCN8a$^{med/+}$ mice (n = 15). (B) Graphs showing changes in the same AP parameters for the last 3 spikes elicited by 300 pA injections before and after CBZ incubation in SCN8a^{WT} (n = 15) and SCN8a$^{med/+}$ mice (n = 15). Statistical significance was determined using a paired t-test. *p < 0.05, **p < 0.01, ****p < 0.0001.

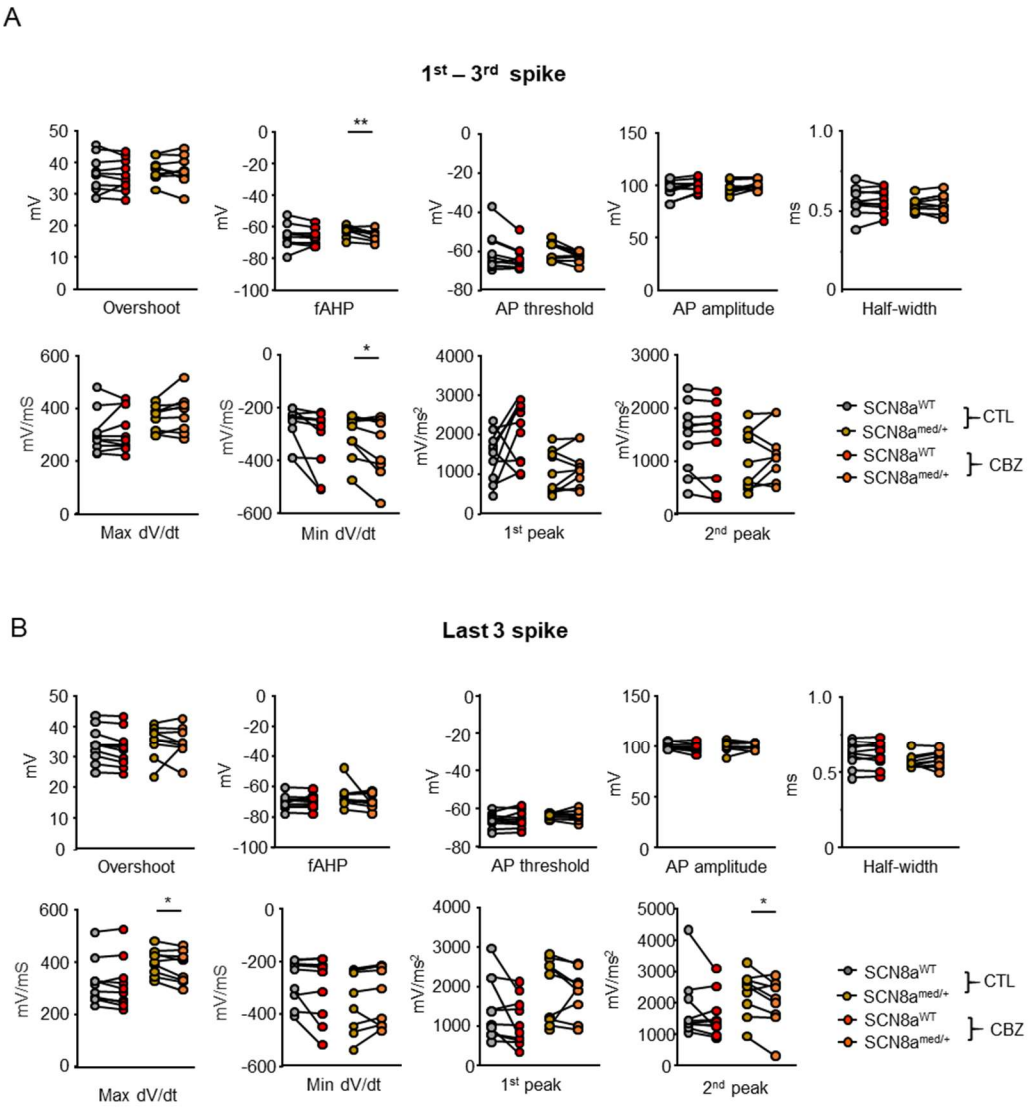

Fig. S11. CBZ-induced changes in parameters of AP elicited by pulse trains in RT Neurons. (A) Graphs showing changes in AP parameters (overshoot, fAHP, AP threshold, AP amplitude, half-width, maximum dV/dt, minimum dV/dt, and 1st /2nd peaks of d²V/dt²) for the 1st–3rd spikes elicited by 50 Hz pulse trains before and after CBZ incubation in SCN8a^{WT} (n = 10) and SCN8a$^{med/+}$ mice (n = 9). (B) Graphs showing changes in the same parameters for the last 3 spikes elicited by 50 Hz pulse trains before and after CBZ incubation in SCN8a^{WT} (n = 10) and SCN8a$^{med/+}$ mice (n = 9). Statistical significance was determined using a paired t-test. *p < 0.05, **p < 0.01.

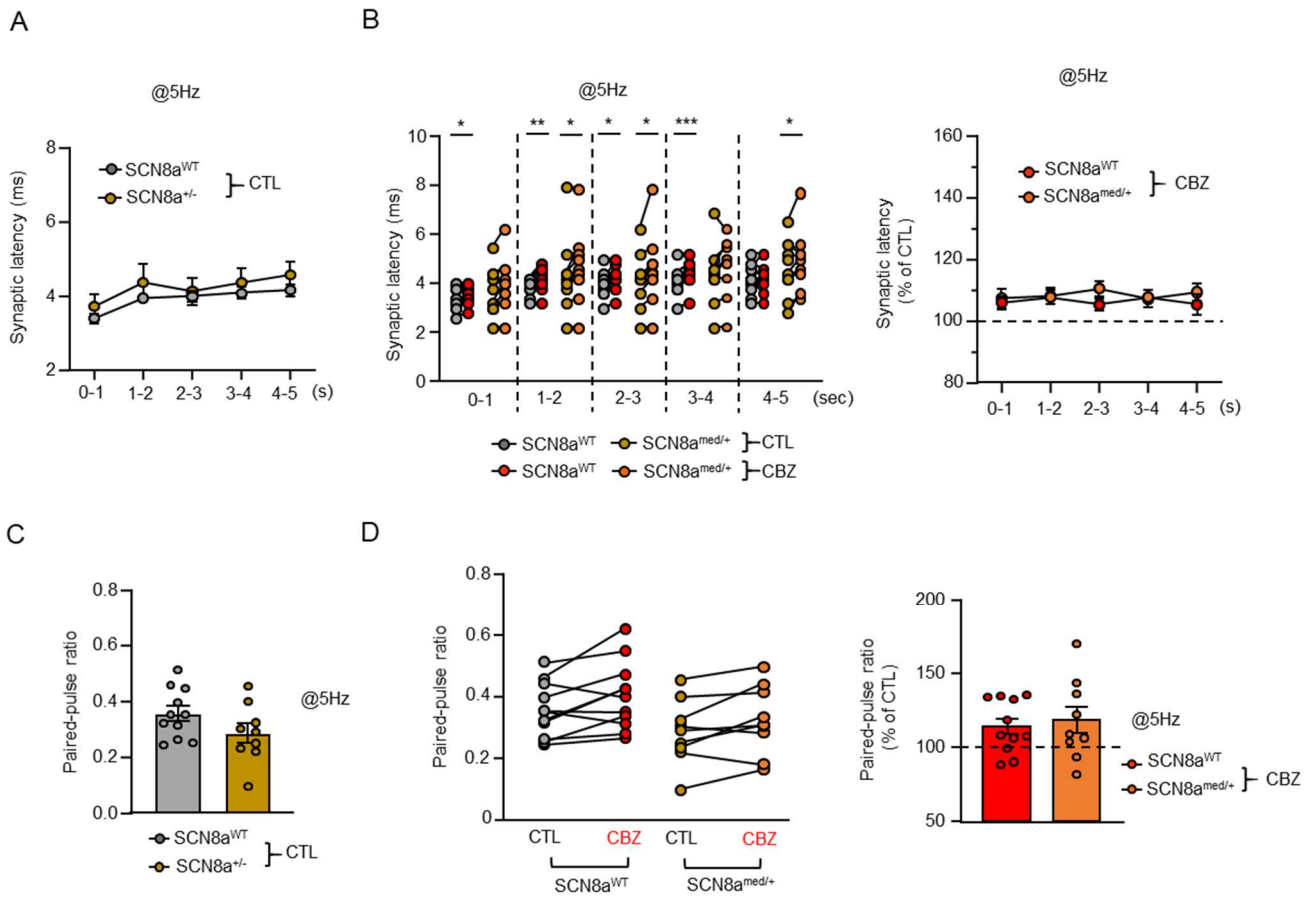

Fig. S12. CBZ Effects on GABAergic Transmission Between SCN8a^{WT} and SCN8a$^{med/+}$ Mice During 5 Hz Stimulation. (A) Graph showing quantified synaptic latency at 1-second intervals before and after CBZ incubation in SCN8a^{WT} (n = 11) and SCN8a$^{med/+}$ mice (n = 9). (B) Graph (left) showing synaptic latency at 1-second intervals and graph (right) showing normalized latency to CTL in response to 5 Hz stimulation in SCN8a^{WT} (n = 11) and SCN8a$^{med/+}$ mice (n = 9) expressing VGAT-ChR2-EYFP. (C) Graph showing the PPR, calculated as the ratio of the 2nd to 1st IPSC peak amplitudes SCN8a^{WT} (n = 11) and SCN8a$^{med/+}$ mice (n = 9). (D) Graph (left) showing the PPR and graph (right) showing normalized PPR to CTL in response to 5 Hz stimulation in SCN8a^{WT} (n = 11) and SCN8a$^{med/+}$ mice (n = 9) expressing VGAT-ChR2-EYFP. Statistical significance was determined using a paired t-test. *p < 0.05, **p < 0.01, ***p < 0.001.

Supplemental material and methods

Viral constructs and injection procedures

For the optogenetic activation experiments, PV-Cre or SOM-Cre mice aged 2 - 3 months underwent stereotaxic injections with AAV5.EF1a.DIO.hChR2(H134R)-eYFP.WPRE.hGH virus under isoflurane anesthesia, with the depth of anesthesia monitored and maintained throughout the procedure. The injections were administered using a microsyringe (10 µL capacity) with a 33-gauge beveled needle (WPI). The stereotaxic coordinates of the injections were 1.1-1.2 mm posterior to Bregma, 1.9-2.1 mm lateral to the midline, 2.8-3.0 depth from the ventral surface. At each site, 300-400 nL of concentrated virus suspension was injected at a rate of 50 nl/min. To prevent backflow, the syringe was left in place for 5 minutes after each injection. The incisions were closed using tissue adhesive (Vetbond, 3M; St.Paul, MN), and the mice were allowed to recover on a heating mat until they became awake.

Optogenetic stimulation

Mice that had previously been injected with AAV5.EF1a.DIO.hChR2(H134R)-eYFP.WPRE.hGH were used in this experiment. Vgat-ChR2 mice and SCN8a-Vgat-ChR2 mice were euthanized, and fresh brain slices were prepared for patch clamp physiology as described above. RT neurons expressing hChR2-eYFP were activated with 475 nm light using a 1.9 mW/cm^2 light source (CoolLED). We applied 1 ms pulses of LED blue light at 5, 10, 20 ,30, and 50 Hz for 5 s to stimulate pre-synaptic release, as previously described (1).

Reference

1. C. D. Makinson, *et al.*, Regulation of Thalamic and Cortical Network Synchrony by Scn8a. *Neuron* **93**, 1165-1179.e6 (2017).